TOPICAL REVIEW — A 40th Anniversary Celebration: Physics Research and Innovation at Ningbo University

Progress in high-pressure hydride superconductors: From theoretical predictions to experimental breakthroughs

Xingbin Zhao(赵行斌)[1,†], Yaqian Dan(但雅倩)[1,†], Haoyang Teng(滕灏洋)[1], Lei Wang(王磊)[1], Wanting Rao(饶婉婷)[1], Yanping Huang(黄艳萍)[1,‡], and Tian Cui(崔田)[1,2]

[1] *Institute of High Pressure Physics, School of Physical Science and Technology, Ningbo University, Ningbo* 315211, *China*
[2] *State Key Laboratory of High Pressure and Superhard Materials, College of Physics, Jilin University, Changchun* 130012, *China*

(Received 11 June 2026; revised manuscript received 9 August 2026; accepted manuscript online 1 September 2026)

The discovery of high-temperature superconductivity in hydrogen-rich compounds at high pressures has reshaped the landscape of condensed matter physics. This review traces the remarkable trajectory of high-pressure hydride superconductors, from early conceptual proposals to recent experimental milestones. We begin with the foundational theoretical framework, including Ashcroft's chemical precompression hypothesis and the electron–phonon coupling mechanism that governs conventional superconductivity in these systems. The central experimental achievements are then examined in chronological order: the record-breaking 203 K transition in H_3S at 155 GPa, the near room-temperature superconductivity at 250–260 K in clathrate-structured LaH_{10}, and other experimentally synthesized binary/ternary hydrides with excellent superconducting properties. We also analyze the unifying structural and electronic features responsible for high transition temperatures. Finally, we address persistent experimental challenges, from unambiguous sample characterization to the definitive detection of the Meissner effect, and outline promising strategies toward the ultimate goal of achieving higher superconducting transition temperatures under lower pressures. This review highlights the powerful synergy between first-principles theory and diamond anvil cell experiments that has driven this field forward.

Keywords: high pressure, hydride, superconductivity, electron–phonon coupling

PACS: 74.62.Fj, 74.25.Dw, 81.05.Zx

DOI: 10.1088/1674-1056/aea0c3 **CSTR:** 32038.14.CPB.aea0c3

1. Introduction

Superconductivity, characterized by the complete disappearance of electrical resistance and the expulsion of magnetic flux below a critical temperature (T_c), has remained one of the most captivating phenomena in physics since its discovery in 1911.[1] The Bardeen–Cooper–Schrieffer (BCS) theory provided a microscopic understanding in 1957, describing how electrons form Cooper pairs through an attractive interaction mediated by lattice vibrations. Within this framework, the critical temperature is governed by the characteristic phonon energy and the strength of the electron–phonon coupling. The search for materials that maximize these parameters has motivated decades of research into high-temperature superconductors.

Elemental hydrogen, owing to its lightest atomic mass, possesses the highest possible Debye temperature among all elements, making metallic hydrogen a theoretically ideal candidate for high-temperature and even room-temperature superconductivity.[2–8] However, the metallization of pure hydrogen is predicted to require pressures exceeding 400–500 GPa,[9–12] placing it at the extreme frontier of static compression techniques. This formidable challenge motivated a paradigm-shifting idea: rather than compressing pure hydrogen, one could incorporate hydrogen into compounds where heavier elements provide an internal chemical pressure, thereby reducing the external pressure required for metallization. In 2004, Ashcroft articulated this concept of chemical precompression, proposing that hydrogen-rich compounds could become metallic and superconducting at pressures far lower than those needed for pure hydrogen.[6] This insight launched a new era in superconductivity research, one in which theory and computation would guide experiment in a tightly coupled feedback loop. Over the subsequent two decades, the combination of advanced first-principles crystal structure prediction methods and ultrahigh-pressure diamond anvil cell techniques has yielded a succession of discoveries that have pushed the superconducting critical temperature from the cryogenic range to nearly ambient temperature. Key milestones include the discovery of superhydrides such as H_3S, which was predicted and then experimentally confirmed to exhibit superconductivity with a T_c of 203 K at 155 GPa, a record at that time.[13–17] More recently, LaH_{10} was found to have a T_c of 250–260 K at pressures around 170–200 GPa, bringing room-temperature superconductivity tanta-

[†]These authors contributed equally to this work.
[‡]Corresponding author. E-mail: huangyanping@nbu.edu.cn

© 2026 Chinese Physical Society and IOP Publishing Ltd. All rights, including for text and data mining, AI training, and similar technologies, are reserved.

CPB Online In Press

lizingly close.[18–21] Notably, relatively high critical temperatures have been reported in cerium- and yttrium-based superhydrides as well. These discoveries have collectively pushed the superconducting critical temperature from the cryogenic range (below 30 K) to within striking distance of ambient temperature.

This review provides a comprehensive account of this journey. We begin by establishing the theoretical principles that guide the search for high T_c hydrides. We then chronicle the key experimental breakthroughs that have defined the field, followed by an analysis of the common physical mechanisms that emerge across different material families. Finally, we offer a summary of current challenges and future directions, which we hope may serve as a useful reference for the broader research community.

2. Theoretical foundations of hydride superconductivity

2.1. The BCS framework and the McMillan equation

Conventional hydride superconductivity is well described by the electron–phonon coupling mechanism, as formalized in BCS theory and its strong-coupling extensions. Grounded in the nearly free electron model, BCS theory was originally formulated for the weak electron–phonon coupling limit. It posits that superconductivity arises from phonon-mediated Cooper pairing, which opens a superconducting energy gap and enables dissipationless charge transport. Hydrogen, owing to its extremely light mass, possesses an exceptionally high Debye temperature. Under high pressure, metallic hydrogen can generate strong electron–phonon coupling, thereby significantly enhancing T_c. Specifically, the extremely light mass of hydrogen leads to very high atomic vibrational frequencies, providing a natural "high-frequency phonon" foundation for achieving high T_c. Under high pressure, the hydrogen-cage structures formed by hydrogen atoms in hydrogen-rich compounds can exhibit a high electronic density of states at the Fermi level, inducing strong electron–phonon coupling. The critical temperature can be estimated using the McMillan formula, which was later refined by Allen and Dynes:[22]

$$T_c = \frac{\omega_{\log}}{1.2} \exp\left[-\frac{1.04(1+\lambda)}{\lambda-\mu^*(1+0.62\lambda)}\right],$$

where $\omega_{\log}$ is the arithmetic mean of the phonon frequencies, λ is the electron–phonon coupling constant, and μ^* is the retarded Coulomb pseudopotential, typically taken to be between 0.1 and 0.15. This equation reveals two essential ingredients for a high T_c: a large characteristic phonon frequency $\omega_{\log}$, naturally provided by the light mass of hydrogen, and a strong coupling constant λ.

2.2. Chemical precompression

In 2004, Ashcroft recognized that the metallization pressure of hydrogen could be substantially reduced by chemically binding hydrogen to other elements.[6] The core idea is elegantly simple: the heavier atoms in a hydride compound exert an internal pressure on the hydrogen sublattice through chemical bonding and steric constraints. This internal pressure precompresses the hydrogen, effectively lowering the external pressure required to drive the system into a metallic state with a high density of states at the Fermi level.

Ashcroft further predicted that such hydrogen-rich compounds, once metallized, would serve as excellent candidates for high-temperature superconductivity. The rationale was twofold. First, the high Debye temperature associated with hydrogen-derived phonon modes sets a favorable energy scale. Second, the electronic states at the Fermi level in these materials are expected to have substantial hydrogen character, ensuring strong modulation of the electronic structure by hydrogen vibrations and hence strong electron–phonon coupling.

2.3. Computational structure prediction

The realization of Ashcroft's vision relied heavily on the development of *ab initio* methods for predicting crystal structures under pressure. Algorithms such as random structure searching, particle swarm optimization, and evolutionary algorithms, combined with density functional theory (DFT) total energy calculations, enabled researchers to systematically explore the energy landscape of binary and ternary hydride systems. These methods not only identify thermodynamically stable and metastable phases but also provide the structural inputs necessary for subsequent phonon and electron–phonon coupling calculations.

This computational infrastructure has transformed the search for superconducting hydrides from a trial-and-error process into a predictive science. Dozens of candidate compounds were computationally identified before being synthesized experimentally, establishing a paradigm in which theory leads and experiment validates.

3. Experimental breakthroughs

3.1. Early investigations

Following Ashcroft's proposal, relatively early experimental and theoretical efforts focused primarily on the group-IVa hydrides, particularly SiH_4. Early theoretical work predicted that SiH_4 would metallize at around 50 GPa and become superconducting.[23] At high pressure, mixed closed shell systems and molecular hydrogen can give rise to novel H_2-containing van der Waals compounds, such as $SiH_4(H_2)_2$ and $GeH_4(H_2)_2$, which have been predicted to be high temperature superconductors with T_c values of 107 K and 90 K at

CPB Online In-Press

250 GPa,[24,25] respectively. Nevertheless, experiments have only observed a low T_c of $\sim$ 17 K for silane at 90 GPa and 120 GPa among these hydrides,[26] although debates persist. These results demonstrated the validity of the chemical precompression concept and encouraged further exploration of higher hydrides with greater hydrogen content.

3.2. The 200 K landmark: H_3S

The year 2015 marked a watershed moment in the field of high-pressure hydride superconductivity. Theoretical calculations by Duan *et al.* predicted that compressed H_2S would decompose into H_3S and elemental sulfur, and that the resulting H_3S phase with a body-centered cubic sulfur sublattice would exhibit a remarkably high T_c of around 200 K at 160 GPa, as shown in Figs. 1(a) and 1(b).[13,14] This prediction was soon experimentally confirmed by Drozdov *et al.*, who synthesized H_3S in a diamond anvil cell and compressed it to approximately 155 GPa. They observed a sharp drop in electrical resistance at 203 K,[16] a value in close agreement with the theoretical predictions, as shown in Figs. 1(c) and 1(d). The structure of H_3S features strong covalent bonding between hydrogen and sulfur, with sulfur adopting a six-fold coordination environment relative to hydrogen.

The discovery was of profound significance for several reasons. First, it shattered the previous record for conventional superconductivity, which had stood for decades. Second, it provided a spectacular validation of the computational prediction pipeline, cementing the role of theory as an equal partner in discovery. Third, it demonstrated that the chemical precompression strategy could yield T_c values well above the boiling point of liquid nitrogen, opening the door to practical cooling technologies. Isotope effect measurements, in which deuterated samples showed a substantially reduced T_c consistent with the BCS prediction, provided further evidence for the phonon-mediated mechanism.

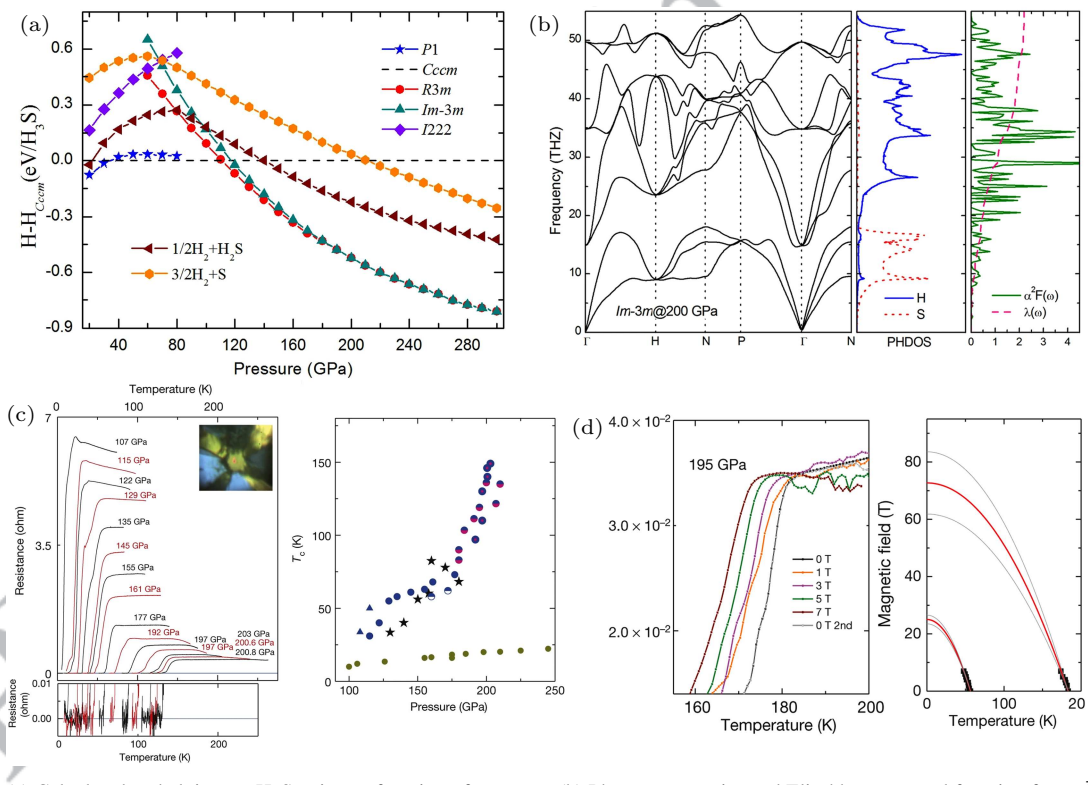


Fig. 1. (a) Calculated enthalpies per H_3S unit as a function of pressure. (b) Phonon properties and Eliashberg spectral function for $Im\bar{3}m$ H_3S at 200 GPa. Adapted with permission from Ref. [13]. (c) Temperature dependence of the resistance of sulfur hydride at different pressures. (d) Temperature dependence of the resistance of sulfur hydride in various magnetic fields, from which the critical magnetic field at 195 GPa is determined. Adapted with permission from Ref. [16].

3.3. The rise of clathrate superhydrides: LaH_{10} and beyond

Following the success of the H–S system, research attention shifted toward a new class of materials known as clathrate superhydrides. In 2012, Wang *et al.* identified the cage-like hydride superconductor CaH_6 and predicted its T_c to be 220–235 K at 150 GPa based on electron–phonon coupling (EPC) calculations,[27] without experimental confirmation at that time, as shown in Fig. 2(a). Subsequently, clathrate compounds based on rare-earth metals garnered substantial research interest. In these compounds, the rare earth atom occupies the center of a polyhedral cage formed by hydrogen atoms, with stoichiometries such as MH_6, MH_9, and MH_{10}. The hydrogen cages exhibit structural motifs analogous to those in classical clathrates, with H_{24}, H_{29}, and H_{32} cages being particularly common. First-principles calculations pre-

dicted extraordinarily high T_c values for several of these materials. Among them, LaH_{10} attracted particular attention, with theoretical estimates suggesting a T_c near room temperature at pressures of around 200 GPa.[18] In 2018–2019, independent experimental groups synthesized LaH_{10} in diamond anvil cells and observed superconducting transitions under pressures of approximately 170–190 GPa. Eremets successfully synthesized LaH_{10}, observing near room temperature superconductivity with a critical temperature of 250–260 K at 150 GPa — a new record for T_c, as shown in Fig. 2(b).[19] In a similar effort, Hemley *et al.* also reported the successful synthesis of superconducting LaH_{10},[20,21] achieving T_c values exceeding 260 K under pressures of 180–200 GPa. The discovery of near room temperature superconductivity in LaH_{10} was a monumental achievement. The measured T_c of 250–260 K is accessible with commercial closed-cycle cryocoolers, making these experiments more widely reproducible and raising the tantalizing prospect of practical applications. Under high pressure, LaH_{10} crystallizes in a clathrate-like structure with sodalite-type symmetry (space group $Fm\bar{3}m$), where lanthanum atoms occupy the framework sites and hydrogen atoms form unusual H_{32} cages featuring both diatomic H_2 units and monatomic hydride ions. This structural motif has since become a hallmark of high-T_c superhydrides.

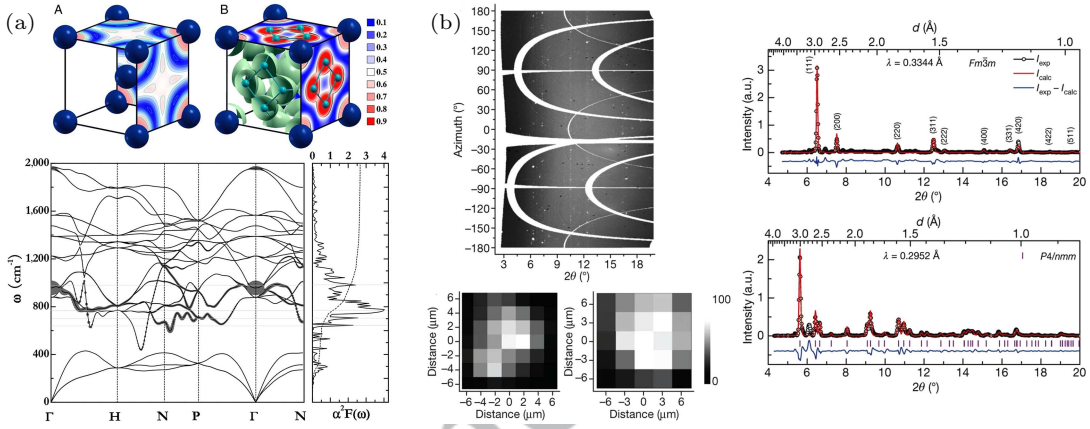


Fig. 2. (a) Electron localization function (ELF), phonon band structure and Eliashberg spectral function of CaH_6 at 150 GPa. Adapted with permission from Ref. [27]. (b) X-ray diffraction studies of experimentally synthesized superconducting lanthanum hydride LaH_{10} at 150 GPa. Adapted with permission from Ref. [19].

Subsequent investigations expanded the family of clathrate superhydrides to include yttrium (YH_6, YH_9),[28,29] cerium (CeH_9, CeH_{10}),[30–32] and thorium (ThH_{10}),[33] among others. Many of these compounds displayed T_c values well above 100 K. Systematic studies began to reveal correlations between T_c, applied pressure, and the hydrogen content and cage topology. Yttrium-based superhydrides have emerged as particularly promising systems due to their multiple stoichiometries and excellent superconducting performances. Comprehensive studies conducted in the pressure range of 140–300 GPa have successfully synthesized a series of yttrium superhydrides including YH_4, YH_6, YH_7, and YH_9. YH_6 exhibits a T_c of 224 K at 166 GPa, making it one of the highest-temperature binary hydride superconductors.[28] The hexagonal structure of YH_6 features hydrogen cages that enable strong electron–phonon coupling, leading to its remarkable superconducting properties. YH_9 demonstrates an even higher T_c of approximately 230–243 K at pressures around 200 GPa.[29] The dense hydrogen framework in YH_9 enhances the density of states at the Fermi level, boosting electron–phonon interactions. Notably, the theoretical prediction of YH_{10} as a potential room-temperature superconductor has not yet been experimentally realized within the studied pressure and temperature ranges (up to 300 GPa and 2000 K).[18]

Cerium-based superhydrides are particularly significant because they stabilize at lower pressures compared to their lanthanum and yttrium counterparts, offering a more accessible pathway for high-temperature superconductivity research. CeH_9, synthesized at pressures of approximately 80–130 GPa,[30–32] exhibits T_c values ranging from 57–100 K.[30] CeH_{10}, a higher hydride synthesized under comparable pressure conditions, demonstrates a T_c of 115 K at 95 GPa.[30] Similarly, ThH_9 and ThH_{10} have also been experimentally synthesized, exhibiting superconducting transition temperatures of 146 K and 161 K, respectively.[33]

CaH_6 represents a particularly important binary cage-like hydride due to its remarkably high T_c. Synthesized at pressures of approximately 160–180 GPa combined with laser heating, CaH_6 crystallizes in the $Im\bar{3}m$ cubic structure. Experimental measurements report a T_c of 215 K at 172 GPa,[34] confirmed by resistance measurements. An important distinguishing feature of CaH_6 is that its T_c exhibits a relatively moderate pressure dependence, suggesting that the superconducting phase remains stable over a wider pressure range compared to lanthanum-based hydrides.

Furthermore, a relatively special class of binary cage-like hydrides is represented by the A15-type La_4H_{23}, which deviates from the common MH_6, MH_9, and MH_{10} stoichiome-

tries. La_4H_{23} adopts an A15 cubic structure (space group $Pm\bar{3}n$), originally known from intermetallic A15 superconductors such as Nb_3Sn. The structure consists of a three-dimensional hydrogen framework with lanthanum atoms occupying two distinct crystallographic sites, forming hydrogen cages of different polyhedral geometries. Unlike conventional MH_{10} clathrates, La_4H_{23} exhibits a metal-to-hydrogen ratio of 4:23, corresponding to approximately 5.75 hydrogen atoms per lanthanum atom. The superconducting properties of La_4H_{23} are remarkable: experimental measurements report a T_c of $\sim$ 105 K at 118 GPa.[35] The A15 structure gives rise to a high density of states at the Fermi level and strong electron–phonon coupling, partly due to the quasi-one-dimensional chains of hydrogen atoms in the lattice. Furthermore, A15-type Lu_4H_{23} has also been reported, with a T_c of 71 K at 218 GPa.[36] In contrast to the more symmetric sodalite-like cages in LaH_{10}, the A15 framework offers an alternative hydrogen bonding network that is equally effective in mediating high-temperature superconductivity.

3.4. Molecular hydrides with H_2 units

Beyond clathrate hydrides, another class of molecular-type hydrides — initially considered unfavorable for high-temperature superconductivity — has also been found to exhibit superconductivity. Early experiments uncovered molecular hydrides such as LiH_6 and NaH_7, in which H_2 units are incorporated and stabilized through ionic interactions with the metal host lattice.[37,38] Despite the absence of observable superconducting transitions in these materials, their structures proved that H_2-based frameworks can remain stable under pressure. Following this, Chen synthesized BaH_{12}, which adopts a pseudo-cubic arrangement with weakly interacting H_2-like motifs that contribute negligibly to the density of states at the Fermi level, resulting in a modest T_c of 20 K at 140 GPa.[39] More recently, BiH_4 was successfully synthesized and shown to exhibit superconductivity with a T_c of 91 K at 170 GPa, establishing it as one of the most promising molecular hydrides achieved experimentally to date.[40] In quasi-H_2-contained hydrides, tightly bound H–H pairs with exceptionally short bond lengths are present, significantly shorter than typical interatomic distances in metallic hydrides, yet slightly longer than those in free gaseous H_2 molecules.[41] Crucially, these H–H pairs are no longer free, neutral H_2 molecules; instead, they are "confined" within the lattice framework formed by metal atoms and act as structural units of the crystal, with their electron clouds interacting with surrounding metal atoms and their vibrational frequencies modulated by the lattice environment. For example, YH_4 also exhibits a similarly high T_c of 88 K at 155 GPa, where hydrogen remains in molecular form rather than as isolated atoms.[42,43] Other quasi-H_2-contained hydrides include SnH_4[44] and YH_7.[43] Based on current experimental results, the clathrate-type hydrogen configuration exhibits superior superconducting properties compared to the molecular-type configuration. This observation aligns with the principle of chemical precompression, which promotes the dissociation of hydrogen molecules into atomic hydrogen, thereby further increasing the proportion of atomic-like hydrogen and enhancing superconducting performance.

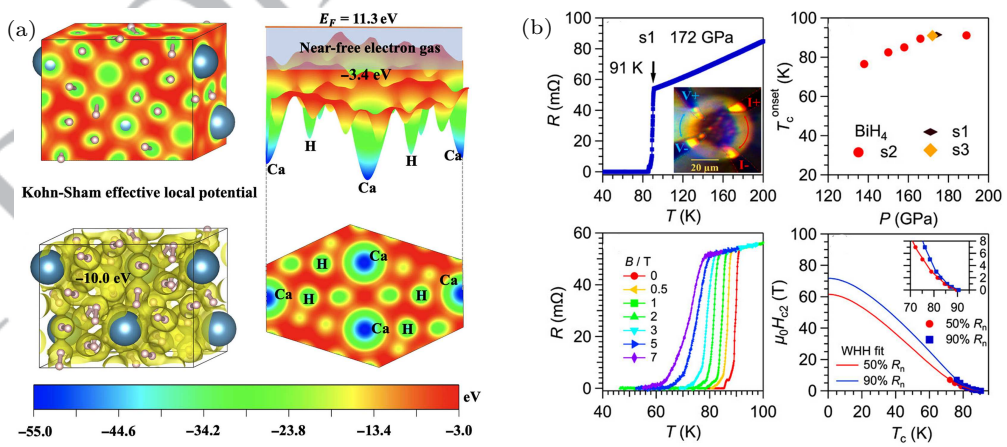


Fig. 3. (a) The Kohn–Sham effective local potential, including ionic, Hartree, and exchange–correlation potentials of $C2/c$-CaH_{14}. Adapted with permission from Ref. [41]. (b) Electrical transport and magnetism of the superconducting molecular hydride BiH_4. Adapted with permission from Ref. [40].

3.5. Extending to ternary hydride systems

The exploration of binary hydrides, while successful in producing high-temperature superconductors, has revealed inherent structural limitations. These compounds typically require stabilization pressures exceeding 150 GPa, and their relatively simple stoichiometries offer limited flexibility for tuning critical parameters, such as electron–phonon coupling and hydrogen sublattice geometry. In response, researchers have increasingly turned to ternary hydride systems incorporating two distinct metal/metalloid species within a hydrogen framework. The expanded compositional space introduces additional degrees of freedom, allowing for the strategic design of

CPL Online In-Press

hydrogen cages and the optimization of electronic properties at more moderate pressure conditions.

Compared to binary hydrides, ternary hydride superconductors offer several distinct advantages arising from their expanded compositional space. First, the introduction of a second metal or metalloid species alleviates the structural constraints inherent in binary systems, enabling the stabilization of hydrogen sublattices at significantly lower external pressures. Second, ternary systems provide additional tuning knobs for optimizing the superconducting critical temperature. By varying the stoichiometry and chemical composition, researchers can systematically enhance the electron–phonon coupling strength and tailor the density of states at the Fermi level — two key factors governing superconductivity. Third, the greater chemical diversity in ternary hydrides often leads to richer hydrogen cage geometries and bonding configurations, which can further boost T_c while maintaining dynamical stability. Finally, many predicted ternary hydrides exhibit metastable behavior, allowing their superconductivity to persist over a broader pressure range, including upon decompression. Collectively, these advantages position ternary hydrides as a more flexible and promising platform for exploring the pathway toward room-temperature superconductivity under experimentally accessible high-pressure conditions, though we recognize that achieving such performance under ambient conditions would require additional stabilization strategies.

In 2021, Semenok *et al.* reported two relatively early examples of ternary high-temperature superconducting hydrides, (La,Y)H_6 and (La,Y)H_{10}.[45] Under pressures of 183–199 GPa, (La,Y)H_{10} achieved a T_c of 245–253 K, whereas (La,Y)H_6 showed a T_c of approximately 237 K. Following these discoveries, alloying strategies were further extended to other rare earth combinations. For instance, the ternary cage-type hydride (La,Ce)H_9 was synthesized under pressures of 110–125 GPa and temperatures of 2100–2300 K.[46,47] This compound achieves a T_c in the range of 148–178 K, which represents an approximately 80% enhancement compared to its binary counterpart CeH_9, and it currently holds the record for the highest known superconducting transition temperature near the megabar pressure range. Additionally, Chen *et al.* introduced an appropriate proportion of Al and synthesized (La,Al)H_{10}, which exhibits a T_c of 178 K at 146 GPa. The upper critical field, fitted using the Werthamer–Helfand–Hohenberg (WHH) model, reaches 223 T under the same pressure.[48]

Among the experimentally synthesized ternary hydride superconductors, $LaBeH_8$ stands out as a particularly significant milestone due to its relatively low stabilization pressure and unique structural chemistry. Structurally, $LaBeH_8$ crystallizes in the face-centered cubic $Fm\bar{3}m$ phase and can be viewed as a rocksalt-type ionic compound of $La^{2+}[BeH_8]^{2-}$, where the $[BeH_8]^{2-}$ unit contains polarized Be–H covalent bonds, as shown in Fig. 4(a).[49] Following theoretical predictions, $LaBeH_8$ was first synthesized in 2023, achieving a T_c of 110 K at a pressure of 80 GPa, substantially lower than the 150–200 GPa typically required for binary hydrides (Fig. 4(b)).[50] The high T_c originates from a high hydrogen-derived density of states at the Fermi level and strong electron–phonon coupling arising from inter-unit H–H vibrations. The unexpected stability at submegabar pressures (down to 80 GPa) stems from the insertion of Be atoms into interstitial regions of the hydrogen sublattice, leading to close packing that stabilizes the system at lower pressures.

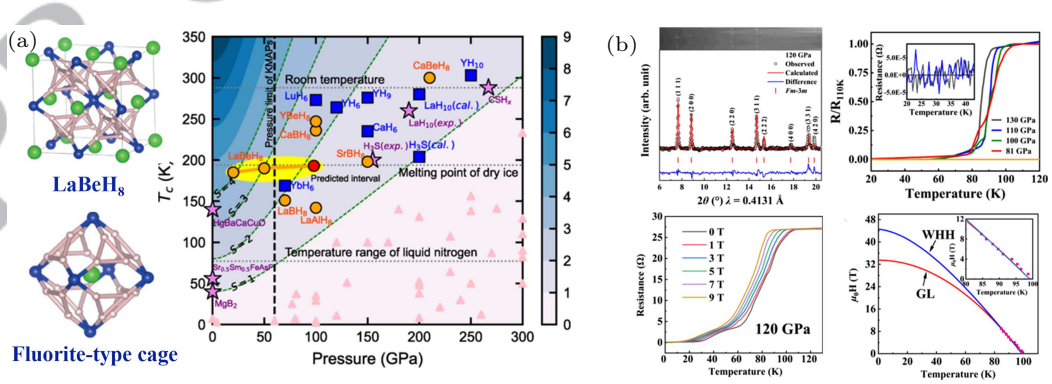


Fig. 4. (a) Crystal structure and pressure dependence of T_c of the $Fm\bar{3}m$ $LaBeH_8$. Adapted with permission from Ref. [49]. (b) Synchrotron x-ray diffraction pattern, temperature dependence of electrical resistance, and critical magnetic field of the $Fm\bar{3}m$ $LaBeH_8$. Adapted with permission from Ref. [50].

A more recent breakthrough involves the successful synthesis of the A15-type ternary hydride $(Lu,Y)_4H_{23}$. This compound exhibits a T_c of 112 K at 215 GPa,[51] which is the highest transition temperature ever recorded for A15-type superconductors and represents a 60% improvement over the binary system. The enhanced performance is attributed to lattice expansion, increased H–H bond lengths, enhanced density of states at the Fermi level, and phonon softening induced by yttrium incorporation. Moreover, the YScH system has also attracted considerable attention. $YScH_8$ was successfully syn-

thesized and found to crystallize in a $P4/mmm$ structure with a T_c of approximately 113 K at 120 GPa, representing an important addition to the family of ternary hydrides based on yttrium and scandium.[52] Collectively, these experimentally realized ternary hydrides including (La,Y)H_6/H_{10},[45] (La,Ce)H_9,[47] (La,Al)H_{10},[48] $LaBeH_8$,[50] $YScH_8$,[52] LaB_2H_8,[53] and so on, demonstrate that expanding from binary to ternary systems offers a powerful strategy for discovering high-temperature superconductors.

In summary, a variety of hydrides with excellent superconductivity have been successfully synthesized experimentally. These hydrides are systematically classified and summarized in Table 1. Figure 5 presents superconducting critical temperatures of various typical hydride superconductors reported experimentally since 2015.

Table 1. Measured superconducting transition temperatures of experimentally reported hydrides under high pressure.

Stoichiometry	Space group	Pressure (GPa)	T_c (K)	Experimental evidence	Ref.
H_3S	$Im\bar{3}m$	155	203	ZR+MFS+IE	[16]
CaH_6	$Im\bar{3}m$	172	215	XRD+ZR+MFS	[34]
YH_6	$Im\bar{3}m$	166	224	XRD+ZR+MFS+IE	[28]
ThH_{10}	$Fm\bar{3}m$	175	161	XRD+ZR+MFS	[33]
CeH_{10}	$Fm\bar{3}m$	95	115	ZR+MFS+XRD+IE	[30]
CeH_9	$P6_3/mmc$	130	100	ZR+MFS+XRD+IE	[30]
ThH_9	$P6_3/mmc$	170	146	XRD+ZR+MFS	[33]
YH_9	$P6_3/mmc$	201	243	XRD+ZR+MFS+IE	[29]
LaH_{10}	$Fm\bar{3}m$	170	250	XRD+ZR+MFS+IE	[19]
La_4H_{23}	$Pm\bar{3}n$	118	105	XRD+ZR+MFS	[35]
Lu_4H_{23}	$Pm\bar{3}n$	218	71	XRD+ZR+MFS	[36]
BiH_4	$C2/c$	170	91	XRD+ZR+MFS	[40]
BiH_2	$Cmcm$	163	62	XRD+ZR+MFS	[54]
(La, Ce)H_9	$P6_3/mmc$	100	176	XRD+ZR+MFS	[47]
(La, Al)H_{10}	$P6_3/mmc$	164	223	XRD+ZR+MFS	[48]
(La, Ca)H_{10}	$P6_3/mmc$	173	247	XRD+ZR+MFS	[55]
(Y, Ce)H_{10}	$Fm\bar{3}m$	149	201	XRD+ZR+MFS+IE	[56]
(La, Y)H_{10}	$Fm\bar{3}m$	183	253	XRD+ZR+MFS	[45]
(Ce, Sc)H_{11}	$Fm\bar{3}m$	190	100	XRD+ZR+MFS	[57]
(La, Ce)$_4H_{23}$	$Pm\bar{3}n$	89	78	XRD+ZR+MFS	[58]
(Lu, Y)$_4H_{23}$	$Pm\bar{3}n$	215	112	XRD+ZR+MFS	[51]
(Y, Ca)H_6	$Im\bar{3}m$	155	224	XRD+ZR+MFS	[59]
$YScH_8$	$P4/mmm$	192	113	XRD+ZR+MFS	[52]
LaB_2H_8	$I4/mmm$	90	106		[53]
$LaBeH_8$	$Fm\bar{3}m$	80	110	XRD+ZR+MFS	[50]

Note: ZR = zero resistance; MFS = magnetic-field suppression; XRD = x-ray diffraction; IE = isotope effect.

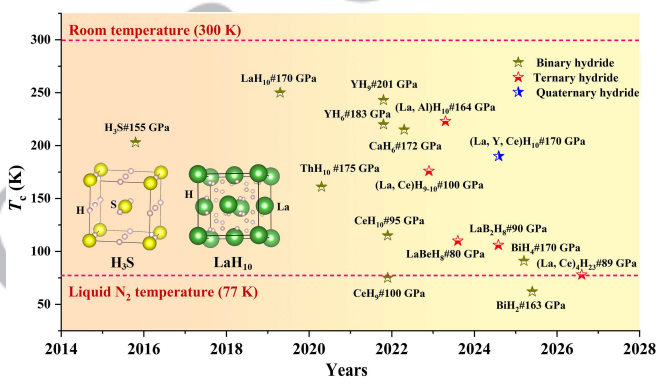


Fig. 5. Experimentally reported superconducting critical temperatures of various hydride superconductors since 2015.

3.6. The gap between theory and experiment

Despite the remarkable experimental successes summarized above, it is important to acknowledge that the theory–experiment feedback loop in this field is not without its unresolved debates. Several systems that are theoretically predicted to be promising remain experimentally elusive. For instance, clathrate hydrides such as YH_{10} and MgH_6 have been extensively predicted to possess excellent superconducting properties,[18,60] yet no superconducting transition has been observed experimentally to date. Perovskite-type hydrides, with $CsInH_3$ as a representative example, which have been theoretically designed to maintain high-temperature superconductivity at relatively lower pressures,[61] have not yet been successfully synthesized or characterized in experiments. Beyond these cases, a broader range of hydride systems have been theoretically predicted to exhibit superconductivity, but no experimental evidence has been found to date.

These gaps between theory and experiment underscore the urgent need for more robust theoretical frameworks that incorporate kinetic pathways, phase competition, and anharmonic effects, as well as for more refined experimental techniques capable of unambiguous phase identification and property characterization under extreme conditions.

Chin. Phys. B Online In-Press

4. Physical mechanisms and universal features

Across the diverse families of superconducting hydrides, a consistent electronic structure picture has emerged. The density of states near the Fermi level is dominated by hydrogen-derived states, primarily from the H 1s orbitals. The metal atoms serve as electron donors, transferring charge to the hydrogen sublattice and stabilizing its structure. This hydrogen-dominated Fermi surface ensures that the electrons responsible for superconductivity are strongly coupled to the hydrogen phonon modes.

The phonon density of states in high-T_c hydrides exhibits a characteristic separation of energy scales. Low-frequency modes are associated with the vibrations of the heavy metal atoms. High-frequency modes, ranging from approximately 100 meV to 250 meV, originate from hydrogen vibrations, including both stretching and librational motions. It is the coupling of electrons to these high-energy hydrogen phonons that provides the dominant contribution to the electron–phonon coupling constant λ.

In clathrate hydrides, the three-dimensional hydrogen cage network gives rise to a high projected density of states from H 1s orbitals at the Fermi level, which strongly enhances the electron–phonon coupling. The Eliashberg spectral function $\alpha^2F(\omega)$ for these systems shows a broad distribution of high-frequency phonon modes with large coupling weights, yielding an electron–phonon coupling constant λ in the range of 1.5–2.5 and a logarithmic average phonon frequency $\omega_{\log}$ exceeding 1000 K. In contrast, molecular-type hydrides such as SnH_4, BiH_4, and YH_4 retain intact H–H or H_2 units, which exhibit more localized molecular vibrations. Their $\alpha^2F(\omega)$ spectra are characterized by sharp peaks at higher frequencies but with substantially lower spectral weight, resulting in λ values typically below 1.0 and $\omega_{\log}$ around 500–800 K. This quantitative difference in clathrate systems directly translates into higher T_c values compared with molecular-type hydrides according to the McMillan–Allen–Dynes formula.

In short, the structural chemistry of hydrogen in these high-pressure phases is remarkably rich. Depending on the pressure, temperature, and chemical composition, hydrogen can exist as isolated H anions, as molecular H_2 units, as extended one-dimensional chains, as two-dimensional layers, or as three-dimensional cage networks. The clathrate cages found in the rare-earth superhydrides represent the most celebrated structural motif, but other configurations are also possible.

5. Current challenges and the path forward

5.1. Experimental hurdles and challenge of evidence standards

Despite the remarkable progress, several formidable experimental challenges persist. The micrometer-scale sample volume within diamond anvil cells at megabar pressures not only complicates the definitive determination of chemical composition and crystal structure, but also fundamentally limits the interpretative power of the most commonly employed measurement. In such confined geometries, a sharp drop in resistance cannot by itself be regarded as a unique signature of bulk superconductivity, although it is a necessary indicator. The superconducting state is characterized by a constellation of interconnected phenomena, including the attainment of truly zero electrical resistance, the expulsion of magnetic flux via the Meissner effect, and perfect diamagnetism. Ideally, these signatures should be observed concurrently on the same sample within the same diamond anvil cell. However, in practice, such comprehensive characterization remains exceptionally difficult at megabar pressures. Furthermore, hydrogen's status as the lightest element makes it a weak x-ray scatterer, thereby complicating the reliable determination of crystal structures via diffraction techniques. Neutron diffraction, though offering superior sensitivity to hydrogen, proves exceedingly challenging to implement under megabar conditions due to the combined constraints of sub-micrometer sample dimensions and insufficient neutron flux.

Despite these challenges, recent technical advances have begun to address the long-standing difficulty of Meissner effect detection in DAC. Conventional approaches, such as AC magnetic susceptibility measurements using miniature pickup coils, have been successfully applied to hydride systems like PtH_x and H_3S, providing evidence of diamagnetic transitions.[17,62] However, these methods face inherent limitations in sensitivity and spatial resolution due to the micrometer-scale sample volumes and strong background signals from the metallic gasket and diamond anvils. A transformative development in this direction is the integration of nitrogen-vacancy (NV) center quantum sensing into DAC platforms. By implanting a thin layer of NV color centers directly into the diamond anvil culet, this technique enables spatially resolved, optical diffraction limited magnetometry at megabar pressures with sub-micron resolution. Crucially, simultaneous transport and magnetic measurements can be performed on the same sample, allowing the direct correlation of zero resistance with the diamagnetic response characteristic of the Meissner effect. This approach has recently been applied to the cerium superhydride CeH_9, where both the Meissner effect and flux trapping were spatially mapped, providing unambiguous evidence of superconductivity.[63]

Taken together, these developments mark a significant step toward establishing more rigorous verification standards for high-pressure superconductivity, and we anticipate that such quantum sensing techniques will play an increasingly central role in the future of the field.

CPB Online In Press

5.2. The path to ambient pressure

The ultimate goal of the field is to realize room-temperature superconductivity at ambient pressure. Achieving this will require stabilizing high-T_c hydride phases under conditions that are thermodynamically or kinetically viable at atmospheric pressure. Several strategies are being actively pursued.

First, ternary and multinary hydride compounds are being explored. The introduction of multiple metal species increases the configurational entropy and can stabilize new crystal structures that may be energetically favorable at lower pressures. Recent discoveries of superconductivity in La–Y–H and La–Ce–H systems at pressures substantially lower than those required for the corresponding binary compounds provide encouraging evidence for this approach.

Second, the substitution of heavier rare earth elements by lighter elements that form strong covalent bonds with hydrogen is being investigated. For example, recent work on $LaBeH_8$ has demonstrated high-temperature superconductivity at pressures that are meaningfully lower than those required for LaH_{10}, suggesting that chemical tuning of the metal–hydrogen interaction can effectively reduce the stabilization pressure.

Third, the concept of metastable retention is being pursued. If a high-pressure superconducting phase can be quenched to ambient conditions and remain kinetically trapped in a metastable state, it may retain its superconducting properties. While this has been demonstrated for some high pressure phases, the rapid diffusion of hydrogen at room temperature presents a formidable obstacle.

5.3. The role of artificial intelligence and high-throughput screening

The vast compositional and structural space of ternary, quaternary, and higher-order hydrides cannot be explored exhaustively with traditional computational methods. Machine learning techniques, including neural network potentials and crystal graph convolutional neural networks, are increasingly being employed to accelerate the search for stable and metastable hydride phases. These tools, combined with high-throughput DFT calculations, are enabling the screening of thousands of candidate compositions and are expected to play a pivotal role in identifying the next generation of high-T_c hydrides.

6. Conclusion

The study of high-pressure hydride superconductors is a remarkable success story in modern condensed matter physics, yet it remains challenging and its full potential is still unfolding. Driven by the interplay of theory and experiment, the field has progressed from the concept of chemical precompression in 2004 to replicated synthesis in specialized high-pressure experiments, and the tantalizing, albeit controversial, claim of room temperature superconductivity. Key unifying features — hydrogen-dominated electronic structures, characteristic phonon spectra, and hydrogen cages — provide a coherent framework for understanding and optimizing these materials. Looking ahead, despite the long and uncertain road from high- pressure discovery to ambient-pressure application, the rapid progress of the past decade offers ample reason for optimism. The integration of advanced computation, innovative synthesis, rigorous characterization, and artificial intelligence promises to accelerate discovery.

Acknowledgements

Project supported by the National Key R&D Program of China (Grant No. 2022YFA1405500) and the National Natural Science Foundation of China (Grant Nos. 52072188 and 12304072).

References

[1] van Delft D and Kes P 2010 *Phys. Today* **63** 38
[2] Ashcroft N W 1968 *Phys. Rev. Lett.* **21** 1748
[3] Azadi S, Monserrat B, Foulkes W M C and Needs R J 2014 *Phys. Rev. Lett.* **112** 165501
[4] Cudazzo P, Profeta G, Sanna A, Floris A, Continenza A, Massidda S and Gross E K U 2008 *Phys. Rev. Lett.* **100** 257001
[5] Monserrat B, Drummond N D, Dalladay S P, Howie R T, Rios P L, Gregoyanz E, Pickard C J and Needs R J 2018 *Phys. Rev. Lett.* **120** 255701
[6] Ashcroft N W 2004 *Phys. Rev. Lett.* **92** 187002
[7] Cudazzo P, Profeta G, Sanna A, Floris A, Continenza A, Massidda S and Gross E K U 2010 *Phys. Rev. B* **81** 134505
[8] Cudazzo P, Profeta G, Sanna A, Floris A, Continenza A, Massidda S and Gross E K U 2010 *Phys. Rev. B* **81** 134506
[9] Dias R P and Silvera I F 2017 *Science* **355** 715
[10] Eremets M I, Drozdov A P, Kong P P and Wang H 2019 *Nat. Phys.* **15** 1246
[11] Loubeyre P, Occelli F and Dumas P 2020 *Nature* **577** 631
[12] Ji C, Li B, Luo J, Zhao Y, Liu Y, Glazyrin K, Bjorling A, Margal L A B, Kahnt M, Kalbfleisch S, Liu W, Gao Y, Wang J, Mao W L, Liu H, Ma Y, Ding Y, Yang W and Mao H K 2025 *Nature* **641** 904
[13] Duan D, Liu Y, Tian F, Li D, Huang X, Zhao Z, Yu H, Liu B, Tian W and Cui T 2014 *Sci. Rep.* **4** 6968
[14] Duan D, Huang X, Tian F, Li D, Yu H, Liu Y, Ma Y, Liu B and Cui T 2015 *Phys. Rev. B* **91** 180502
[15] Li Y, Hao J, Liu H, Li Y and Ma Y 2014 *J. Chem. Phys.* **140** 174712
[16] Drozdov A P, Eremets M I, Troyan I A, Ksenofontov V and Shylin S I 2015 *Nature* **525** 73
[17] Huang X, Wang X, Duan D, Sundqvist B, Li X, Huang Y, Yu H, Li F, Zhou Q, Liu B and Cui T 2019 *Natl. Sci. Rev.* **6** 713
[18] Liu H, Naumov L, Hoffmann R, Ashcroft N W and Hemley R J 2017 *Proc. Natl. Acad. Sci. USA* **114** 6990
[19] Drozdov A P, Kong P P, Minkov V S, Besedin S P, Kuzovnikov M A, Mozaffari S, Balicas L, Balakirev F F, Graf D E, Prakapenka V B, Greenberg E, Knyazev D A, Tkacz M and Eremets M I 2019 *Nature* **569** 528
[20] Somayazulu M, Ahart M, Mishra A K, Geballe Z M, Baldini M, Meng Y, Struzhkin V V and Hemley R J 2019 *Phys. Rev. Lett.* **122** 027001
[21] Geballe Z M, Liu H, Mishra A K, Ahart M, Somayazulu M, Meng Y, Baldini M and Hemley R J 2018 *Angew. Chem. Int. Ed.* **57** 688
[22] Allen P B and Dynes R C 1975 *Phys. Rev. B* **12** 905

CPB Online In Press

[23] Chen X J, Wang J L, Struzhkin V V, Mao H K, Hemley R J and Lin H Q 2008 *Phys. Rev. Lett.* **101** 077002

[24] Li Y W, Gao G Y, Xie Y, Ma Y M, Cui T and Zou G T 2010 *Proc. Natl. Acad. Sci. USA* **107** 15708

[25] Zhong G H, Zhang C, Chen X J, Li Y L, Zhang R Q and Lin H Q 2012 *J. Phys. Chem. C* **116** 5225

[26] Eremets M I, Troyan I A, Medvedev S A, Tse J S and Yao Y 2008 *Science* **319** 1506

[27] Wang H, Tse J S, Tanaka K, Iitaka T and Ma Y 2012 *Proc. Natl. Acad. Sci. USA* **109** 6463

[28] Troyan I A, Semenok D V, Kvashnin A G, Sadakov A V, Sobolevskiy O A, Pudalov V M, Ivanova A G, Prakapenka V B, Greenberg E, Gavriliuk A G, Lyubutin I S, Struzhkin V V, Bergara A, Errea I, Bianco R, Calandra M, Mauri F, Monacelli L, Akashi R and Oganov A R 2021 *Adv. Mater.* **33** 2006832

[29] Kong P, Minkov V S, Kuzovnikov M A, Drozdov A P, Besedin S P, Mozaffari S, Balicas L, Balakirev F F, Prakapenka V B, Chariton S, Knyazev D A, Greenberg E and Eremets M I 2021 *Nat. Commun.* **12** 5075

[30] Chen W, Semenok D V, Huang X, Shu H, Li X, Duan D, Cui T and Oganov A R 2021 *Phys. Rev. Lett.* **127** 117001

[31] Salke N P, Davari E M M, Zhang Y, Kruglov L A, Zhou J, Wang Y, Greenberg E, Prakapenka V B, Liu J, Oganov A R and Lin J F 2019 *Nat. Commun.* **10** 4453

[32] Li X, Huang X, Duan D, Pickard C J, Zhou D, Xie H, Zhuang Q, Huang Y, Zhou Q, Liu B and Cui T 2019 *Nat. Commun.* **10** 3461

[33] Semenok D V, Kvashnin A G, Ivanova A G, Svitlyk V, Fominski V Y, Sadakov A V, Sobolevskiy O A, Pudalov V M, Troyan I A and Oganov A R 2020 *Mater. Today* **33** 36

[34] Ma L, Wang K, Xie Y, Yang X, Wang Y Y, Liu H Y, Yu X H, Zhao Y S, Wang H B, Liu G T and Ma Y M 2022 *Phys. Rev. Lett.* **128** 167001

[35] Guo J N, Semenok D, Shutov G, Zhou D, Chen S, Wang Y L, Zhang K X, Wu X Y, Luther S, Helm T, Huang X L and Cui T 2024 *Natl. Sci. Rev.* **11** nwae149

[36] Li Z, He X, Zhang C, Lu K, Min B, Zhang J, Zhang S, Zhao J, Shi L, Peng Y, Feng S, Deng Z, Song J, Liu Q, Wang X, Yu R, Wang L, Li Y, Bass J D, Prakapenka V, Chariton S, Liu H and Jin C 2023 *Sci. China Phys. Mech. Astron.* **66** 267411

[37] Pépin C, Loubeyre P, Occelli F and Dumas P 2015 *Proc. Natl. Acad. Sci. USA* **112** 7673

[38] Struzhkin V V, Kim D Y, Stavrou E, Muramatsu T, Mao H K, Pickard C J, Needs R J, Prakapenka V B and Goncharov A F 2016 *Nat. Commun.* **7** 12267

[39] Chen W, Semenok D V, Kvashnin A G, Huang X, Kruglov I A, Galasso M, Song H, Duan D, Goncharov A F, Prakapenka V B, Oganov A R and Cui T 2021 *Nat. Commun.* **12** 273

[40] Shan P, Ma L, Yang X, Li M, Liu Z, Hou J, Jiang S, Zhang L, Shi L, Yang P, Lin C, Wang B, Sun J, Guo H, Ding Y, Gou H, Zhao Z and Cheng J 2024 *J. Am. Chem. Soc.* **147** 4375

[41] Liu P Y, Zhuang Q, Xu Q, Cui T and Liu Z 2025 *Sci. Adv.* **11** eadt9411

[42] Wang Y, Wang K, Sun Y, Ma L, Wang Y C, Zou B, Liu G T, Zhou M and Wang H B 2022 *Chin. Phys. B* **31** 106201

[43] Shao M, Chen W, Zhang K, Huang X and Cui T 2021 *Phys. Rev. B* **104** 174509

[44] Troyan I A, Semenok D V, Ivanova A G, Sadakov A V, Zhou D, Kvashnin A G, Kruglov I A, Sobolevskiy O A, Lyubutina M V, Perekalin D S, Helm T, Tozer S W, Bykov M, Goncharov A F, Pudalov V M and Lyubutin I S 2023 *Adv. Sci.* **10** 2303622

[45] Semenok D V, Troyan I A, Ivanova A G, Kvashnin A G, Kruglov I A, Hanfland M, Sadakov A, Sobolevskiy O A, Pervakov K S, Lyubutin I S, Glazyrin K, Giordano N, Karimov D N, Vasiliev A L, Akashi R, Pudalov V M and Oganov A R 2021 *Mater. Today* **48** 18

[46] Bi J, Nakamoto Y, Zhang P, Shimizu K, Zou B, Liu H Y, Zhou M, Liu G T, Wang H B and Ma Y M 2022 *Nat. Commun.* **13** 5952

[47] Chen W, Huang X, Semenok D, Chen S, Zhou D, Zhang K, Oganov A and Cui T 2023 *Nat. Commun.* **14** 2660

[48] Chen S, Qian Y, Huang X, Chen W, Guo J, Zhang K, Zhang J, Yuan H and Cui T 2024 *Natl. Sci. Rev.* **11** nwad107

[49] Zhang Z H, Cui T, Hutcheon M J, Shipley A M, Song H, Du M Y, Kresin V Z, Duan D F, Pickard C J and Yao Y S 2022 *Phys. Rev. Lett.* **128** 047001

[50] Song Y, Bi J, Nakamoto Y, Shimizu K, Liu H, Zou B, Liu G, Wang H and Ma Y 2023 *Phys. Rev. Lett.* **130** 266001

[51] Zhang K, Yu J, Zhang Y, Guo J, Wang Y, Jiang C, Huang X and Cui T 2025 *J. Am. Chem. Soc.* **147** 11879

[52] Jia W, Lv X, Huang Y, Gu Q, He D, Hu K, Zhao X, Zhang Z, Huang Y and Cui T 2026 *Phys. Rev. B* **113** 144507

[53] Song X, Hao X, Wei X, He X, Liu H, Ma L, Liu G, Wang H, Niu J, Wang S, Qi Y, Liu Z, Hu W, Xu B, Wang L, Gao G and Tian Y 2024 *J. Am. Chem. Soc.* **146** 13797

[54] Ma L, Yang X, Li M, Shan P, Liu Z, Hou J, Jiang S, Zhang L, Lin C, Yang P, Wang B, Sun J, Ding Y, Gou H, Guo H and Cheng J 2025 *Phys. Rev. Lett.* **135** 226003

[55] Chen S, Guo J, Wang Y, Wu X, Chen W, Huang X and Cui T 2024 *Phys. Rev. B* **109** 224510

[56] Yang Y, Wang Z, Zhou M, Bi J, Sui Y, Zou B, Liu H, Liu G, Wang H and Ma Y 2026 *J. Am. Chem. Soc.* **148** 21580

[57] Chen Y, Jia X, Wang H, Li Q, Yao Y, Zhou M, Wang H, Liu G and Ma Y 2026 *Sci. Bull.* **71** 2682

[58] Wang Y, Guo J, Chen S, Zhang K, Cui T and Huang X 2026 *J. Am. Chem. Soc.* **148** 24000

[59] Zhang K, Guo J, Wang Y, Wu X, Huang X and Cui T 2025 *Chin. Phys. Lett.* **42** 110704

[60] Feng X L, Zhang J R, Gao G Y, Liu H Y and Wang H 2015 *RSC Adv.* **5** 59292

[61] Du M Y, Huang H Y, Zhang Z H, Wang M, Song H, Duan D F and Cui T 2024 *Adv. Sci.* **11** 2408370

[62] Matsuoka T, Hishida M, Kuno K, Hirao N, Ohishi Y, Sasaki S, Takahama K and Shimizu K 2019 *Phys. Rev. B* **99** 144511

[63] Bhattacharyya P, Chen W, Huang X, Chatterjee S, Huang B, Kobrin B, Lyu Y, Smart T J, Block M, Wang E, Wang Z, Wu W, Hsieh S, Ma H, Mandyam S, Chen B, Davis E, Geballe Z M, Zu C, Struzhkin V, Jeanloz R, Moore J E, Cui T, Galli G, Halperin B I, Laumann C R and Yao N Y 2024 *Nature* **627** 73

CPB Online In Press